Proceedings of 4th ICAPM
August 10–12, 2009, Istanbul, TURKEY
6

THE FLOW OF SATURATED VAPORS THROUGH POROUS VYCOR GLASS

Thomas Loimer*, Petr Uchytil, Roman Petrickovic, Kateřina Setnicková
Institute of Fluid Mechanics and Heat Transfer, Vienna University of Technology, 1040 Vienna, Austria
Institute of Chemical Process Fundamentals, Academy of Sciences of the Czech Republic, Czech Republic
*Correspondence author: Fax: +43 1 58801 32299, Email: thomas.loimer@tuwien.ac.at

ABSTRACT

The flow of saturated vapors and of vapors close to saturation through porous Vycor glass with pore diameters between 10 nm and 200 nm is investigated theoretically and experimentally. The flow process is described assuming an adiabatic flow, accounting for the Joule-Thomson effect and solving the balances of mass, momentum and energy. The experimental data corroborates a former analytical result: Even when capillary condensation is possible, a vapor close to saturation or a saturated vapor only condenses fully when the permeability of the membrane is lower than a critical permeability.

NOMENCLATURE

$k_{\mathrm{m,l}}$	effective thermal conductivity of the liquid-filled membrane (W/mK)
L	membrane thickness (m)
p_{cap}	capillary pressure (Pa), cf. eq. (5)
p_{K}	equilibrium vapor pressure at a curved meniscus (Pa), cf. eq. (4)
p_{lg}	saturation pressure (Pa)
r	pore radius (m)
β	molecular flow factor, cf. eq. (3)
κ	permeability (m^2), cf. eq. (2)
κ_{c}	critical permeability (m^2), cf. eq. (7)
ν_{app}	apparent kinematic viscosity of the vapor (m^2/s), cf. eq. (3)
τ	tortuosity, cf. eq. (2)

INTRODUCTION

The flow of fluids through porous media is a topic that has received long and continuing interest [1–3]. Here, we consider the flow of a vapor close to saturation through a porous membrane which is wetted by the liquid phase of the fluid. The vapor may condense, either due to capillary condensation or due to the Joule-Thomson effect [4]. Hence, liquid, vapor, or a two-phase mixture may flow through parts or all of the membrane, and the flow process becomes quite intricate [5]. The pore sizes of the porous material under investigation are so small that capillary forces at fronts of phase change play an important role. Due to the large amount of heat transported to or from fronts of phase change it may be appropriate to describe the heat transfer at these fronts under thermal non-equilibrium conditions [6]. In this work, we consider capillary forces, real gas properties of the vapor, and we assume local thermodynamic equilibrium everywhere.

Rhim & Hwang [7] investigated the flow of vapors through porous Vycor glass with pore diameters of approximately 4 nm. They mentioned that the heat of vaporization that is released or consumed at the locations of phase change leads to a temperature gradient in the flow field, even if care is taken to keep the system isothermal. However, usually the flow is described assuming an isothermal flow field [8–10].

Schneider [4] pointed out that a vapor close to saturation, regardless of the wetting properties of the materials involved, may also condense due to the Joule-Thomson effect. Schneider proposed that, for condensation to occur, the permeability of the membrane must be smaller than a critical permeability, see eq. (8) in Ref. [4]. He assumed adiabatic conditions and described the flow accounting for the transport of heat. Later, his description was extended by considering also the wetting properties between the fluid and the membrane material [11].

Here, we investigate the flow of vapors through porous glass membranes with pore sizes between 10 nm and 200 nm. The porous medium is modeled

as a bundle of parallel, round tubes and an adiabatic description of the flow is compared with experimental data.

THEORETICAL DESCRIPTION

The mass flux of a vapor far from saturation through a porous membrane is estimated by the mass flux for an ideal gas,

$$\dot{m}_\mathrm{g} = \frac{\kappa}{L}\frac{p_1 - p_2}{\nu_\mathrm{app}(T_1, (p_1 + p_2)/2)}, \quad (1)$$

where the permeability of the membrane is given by

$$\kappa = (\varepsilon/\tau)(r^2/8). \quad (2)$$

If the pore space of a membrane consisted entirely of cylindrical, straight pores, the tortuosity τ would be equal to 1. To account for contributions to the mass transport due to both viscous and molecular flow, the apparent viscosity of the gas or the vapor is given by

$$\nu_\mathrm{app} = \nu_\mathrm{g}(1 + \beta\mathrm{Kn})^{-1}. \quad (3)$$

The Knudsen number is calculated by estimating the mean free path from kinetic gas theory, $\bar{\lambda} = 3\nu_\mathrm{g}\sqrt{\pi/(RT)}$. Ideally, for molecular flow through a round, straight tube, the factor β in eq. (3) would be equal to 8.1.

The mass flux given by eq. (1) is used as a reference throughout the present work. For all experimental and theoretical data points the mass flux is calculated according to eq. (1), and all results are presented in terms of the mass flux ratio $\dot{m}/\dot{m}_\mathrm{g}$.

For the isothermal and the adiabatic description of the flow ideal wetting, i.e., a contact angle of $\theta = 0$, is assumed. According to the isothermal description of the flow, the vapor condenses for $p_1 \geq p_\mathrm{K}$, but remains in its gaseous state for $p_1 \leq p_\mathrm{K}$. Here, p_K is given by Kelvin's equation,

$$\ln(p_\mathrm{K}/p_\mathrm{lg}) = -p_\mathrm{cap}v_\mathrm{l}/(RT_1), \quad (4)$$

and it is the pressure of the vapor in equilibrium with its liquid phase above a meniscus with a radius of curvature equal to the pore radius r, at the temperature T_1. The pressure difference between the gaseous and the liquid phase across the beforementioned meniscus is given by

$$p_\mathrm{cap} = 2\sigma\cos\theta/r. \quad (5)$$

Hence, for $p_1 > p_\mathrm{K}$ the mass flux is given by [10]

$$\dot{m} = \frac{\kappa}{L}\left(\frac{p_\mathrm{K} - p_2}{\nu_\mathrm{app}(T_1, (p_\mathrm{K} + p_2)/2)} + \frac{p_1 - p_\mathrm{K} + p_\mathrm{cap}(p_1 - p_\mathrm{K})/(p_\mathrm{lg} - p_\mathrm{K})}{\nu_\mathrm{l}}\right), \quad (6)$$

which is much larger than the mass flux of an ideal gas. See Fig. 1a for the sketch of the flow in a single pore for $p_1 = p_\mathrm{lg}$ under isothermal flow conditions.

In the adiabatic description of the flow, the mass flux is calculated numerically. The downstream state of the fluid is calculated from the thermic and caloric properties of the vapor by using the Joule-Thomson coefficient. Darcy's law is assumed to hold locally and the mass and energy balances are satisfied. Properties of the fluid, depending on temperature and on pressure, are given by correlations from literature containing up to five parameters. The numerical procedure is similar to that given in Ref. [12].

For $p_1 = p_\mathrm{lg}$, linearized descriptions of the adiabatic flow exist for $\theta = 0$ [11] and $\theta = \pi/2$ [4]. In Ref. [11] the possible flow configurations for arbitrary contact angles, pressure differences and permeabilities are presented. An important result from the linearized description is that a critical permeability κ_c exists [4],

$$\kappa_\mathrm{c} = \frac{\nu_\mathrm{l}k_\mathrm{m,l}}{\Delta h_\mathrm{lg}\mathrm{d}p_\mathrm{lg}/\mathrm{d}T}, \quad (7)$$

where $k_\mathrm{m,l}$ is the effective thermal conductivity of the liquid-filled membrane.

For a permeability of the membrane larger than the critical permeability, the fluid condenses partially and a two-phase mixture flows through part or all of the membrane. In this case the adiabatic description of the flow predicts a mass flux which is very well approximated by that of an ideal gas. For $\kappa < \kappa_\mathrm{c}$ the fluid condenses fully and liquid flows through part or all of the membrane. In that case, capillary action may substantially increase the mass flux with respect to $\dot{m}_\mathrm{g}$.

In Fig. 1b, the flow configuration in a single pore is sketched according to the adiabatic description for $p_1 = p_\mathrm{lg}$ and $\kappa < \kappa_\mathrm{c}$. In Fig. 1, the pressure differences across a meniscus is indicated by the curvature of the meniscus. Note, that according to the isothermal description the meniscus at the upstream side is plane, while according to the adiabatic description it is curved. When adiabatic conditions are assumed, the heat released by evaporation at the upstream meniscus causes an increase in temperature, hence the vapor in front of the upstream meniscus is not fully saturated.

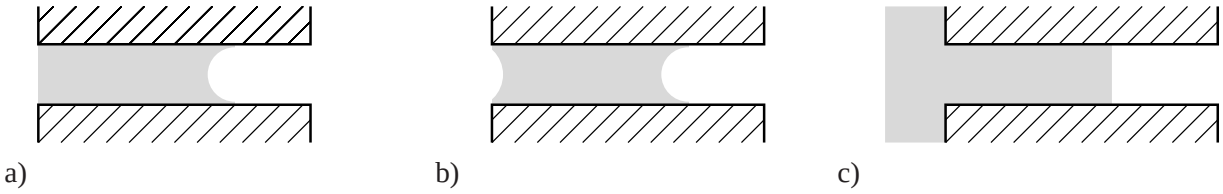

Figure 1

Sketch of the flow in a single pore for $p_1 = p_{lg}$. Flow from left to right. Grey areas stand for liquid. (a) Isothermal flow, $\theta = 0$, (b) adiabatic flow, $\theta = 0$, (c) adiabatic flow, $\theta = \pi/2$.

EXPERIMENTS

The flux of vapors of butane and isobutane through porous Vycor glass membranes was measured. Membranes with pore diameters of 100 nm and 200 nm (Shirasu porous glass, SPG Technology Co., Ltd., Miyazaki, Japan) and between 11 nm and 150 nm (ChemiePark Institut GmbH, Bitterfeld, Germany) were used. Pore sizes were determined with mercury porosimetry. Pore size distributions with a standard deviation of around 10% of the mean were found. The membranes were in circular shape with an outer diameter of approximately 20 mm and thicknesses of either 0.5 mm or 1 mm.

Fluxes were measured using a steady state permeation method. A permeation cell was made from polyvinylchloride to decrease the heat transfer between the fluid and the environment. Each membrane sample was glued with epoxy resin into a circular membrane holder. These membrane holders could then be placed between the two parts of the permeation cell.

Bottles containing nitrogen, butane or isobutane were connected to the upstream side of the permeation cell. On both sides of the membrane, the pressure could be adjusted by pressure regulation valves (Brooks Instrument, Hatfield, USA). However, to conduct measurements with saturated or nearly saturated vapors, the upstream valve between the permeation cell and the butane or isobutane bottle was fully opened. The gas flow was measured with a soap film flow meter at atmospheric conditions, downstreams of the downstream pressure regulation valve. The accuracy of the measurements decreases with decreasing the pressure difference across the membranes. For pressure differences smaller than about 30 kPa, about 10 minutes and up to 30 minutes were allowed to reach steady state before taking a measurement.

Mass flow data for nitrogen was used to determine the tortuosity τ and the molecular flow correction factor β for each membrane, see eqs. (2) and (3). The tortuosities ranged between 0.77 and 1.33, β between 3.83 and 9.62. The small and even unphysical values for the tortuosity are owed to the different sampling of the pore space in mercury porosimetry and in a permeation experiment [13].

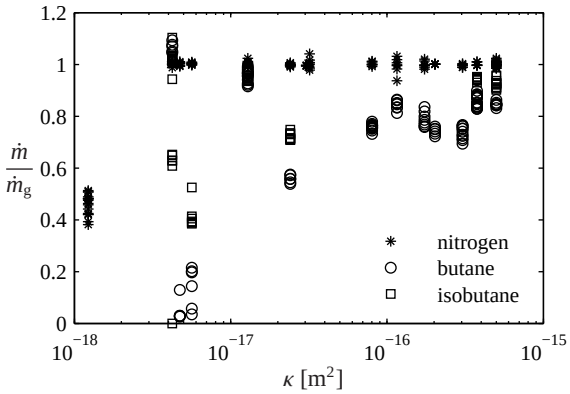

Figure 2

Mass flux of nitrogen and of unsaturated vapors through membranes with different permeabilities. In the graph, 136 measurements for nitrogen and 183 measurements for unsaturated vapors with $p_1 < p_{lg} - 2(p_{lg} - p_K)$ are shown.

Table 1
Topological properties of selected membranes.

κ [m^2]	pore dia. [nm]	ε
1.23×10^{-18}	11	0.32
1.29×10^{-17}	33	0.36
8.03×10^{-17}	95	0.33
2.03×10^{-16}	100	0.50
5.00×10^{-16}	200	0.50

Figure 2 shows the mass flux of nitrogen and of unsaturated vapors, $p_1 < p_{lg} - 2(p_{lg} - p_K)$, versus the permeability of the membranes. For convenience, permeabilities and pore sizes of some membranes are given in Table 1. Since the nitrogen data was used to deter-

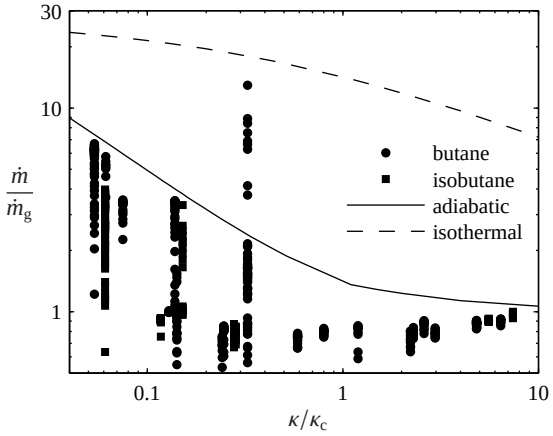

Figure 3

Mass flux for saturated vapors and for vapors close to saturation, $p_1 > p_K$. The solid and the dashed lines refer to calculations with $p_1 = (p_{lg} + p_K)/2$ and $p_1 - p_2 = 50$ kPa. In the graph, 540 measurements are shown. 10 additional data points with $\dot{m}/\dot{m}_g < 0.5$ are not visible.

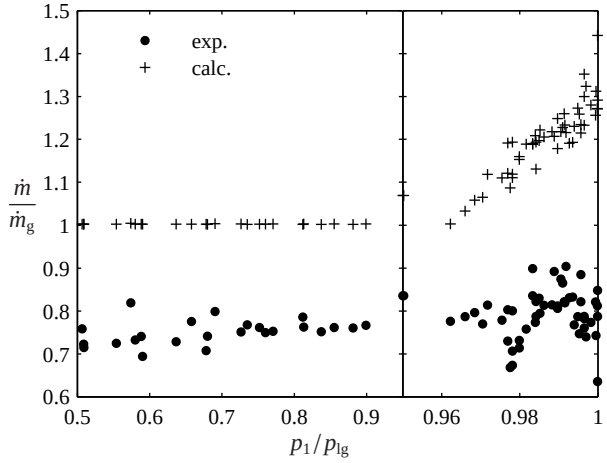

Figure 4

Mass flux versus reduced pressure for $2 < \kappa/\kappa_c < 4$. Here, $p_K/p_{lg} \approx 0.983$. Data from 75 measurements is plotted.

mine independently τ and β for each membrane, the nitrogen data is closely collected around $\dot{m}/\dot{m}_g = 1$. There is one exception, the membrane with a pore diameter $2r = 11$ nm gave mass flow rates which were an order of magnitude lower than expected. In Fig. 2, the data for this membrane, at $\kappa = 1.2 \times 10^{-18}$ m^2, is plotted by calculating $\dot{m}_g$ with $\beta = 0.25$. This value of β compares very unfavourably with the values of β for the other membranes. Nevertheless, the measured values are approximately half the calculated values. Therefore, data for this membrane was excluded from further analysis.

Fig. 2 shows that the mass flux for unsaturated butane and isobutane vapors is, in general, about 80% of the mass flux which is obtained assuming an ideal gas. It seems that the mass flux of vapors, even far from saturation, is reduced with respect to the mass flux of a non-condensable gas. We take the 20% difference as the accuracy obtainable with our simple description. However, for two membranes with permeabilities of about 5×10^{-18} m^2, mass flux ratios smaller than 0.5 were measured. Data around $\kappa/\kappa_c \approx 0.06$, which is the value corresponding to these two membranes, was analyzed previously [14]. Measurements with $\dot{m}/\dot{m}_g < 0.6$ were taken at pressure differences less than 30 kPa [14].

RESULTS

In Fig. 3 the mass flux for vapors close to saturation, $p_1 > p_K$, is plotted versus the permeability divided by the critical permeability κ/κ_c, cf. eqs. (2) and (7). In our experiments, the critical permeability had values in the range between 6.8×10^{-17} m^2 and 1.4×10^{-16} m^2, which corresponds to pore diameters between 86 and 124 nm.

Fig. 3 also shows the mass flux ratio calculated for an upstream condition close to saturation, $p_1 = (p_{lg} + p_K)/2$, and a pressure difference of $p_1 - p_2 = 50$ kPa. The solid and the dashed line correspond to the adiabatic and the isothermal description of the flow, respectively. Fig. 3 shows that, as long as the permeability of the membrane is larger than approximately half the critical permeability, the mass flux of vapors close to saturation or far from saturation is nearly the same. This behavior is qualitatively reproduced by the adiabatic description of the flow, but not by the isothermal description. For $\kappa/\kappa_c < 0.5$, the mass flux ratio is considerably increased.

We now turn to Figs. 4 to 6, which show the mass flux ratio versus the reduced pressure p_1/p_{lg} for narrow ranges of permeabilities. In Figs. 4 to 6, the black dots refer to the experimental data. To every experimental data point corresponds a computed point, marked by a cross, which is calculated according to the adiabatic description for exactly the same conditions under which the measurement was taken. Note that in Figs. 4 to 6 the scale on the abscissa changes at

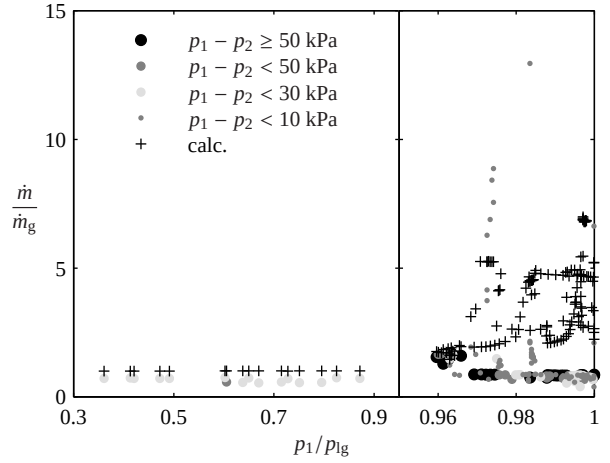

Figure 5
Mass flux versus reduced pressure for $0.2 < \kappa/\kappa_c < 0.4$. Here, $p_K/p_{lg} \approx 0.98$. The experimental data is color-coded by the pressure difference. A total of 162 measurements are shown.

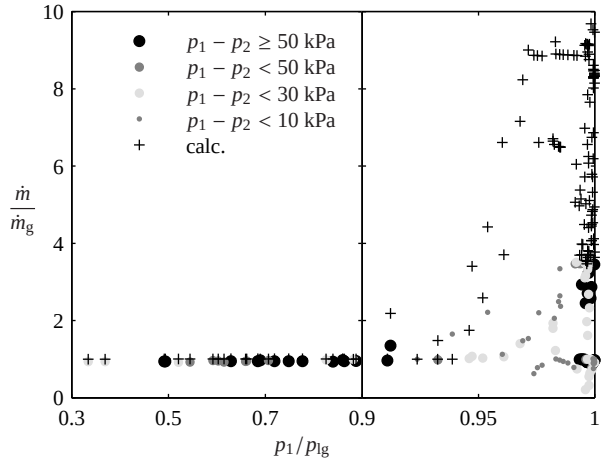

Figure 6
Mass flux versus reduced pressure for $0.1 < \kappa/\kappa_c < 0.2$. Here, $p_K/p_{lg} \approx 0.945$. The experimental data is color-coded by the pressure difference. 136 measurements are plotted.

the vertical line in the graphs.

For $2 < \kappa/\kappa_c < 4$, see Fig. 4, the mass flux ratio is nearly independent of the reduced pressure. For the data plotted in Fig. 4, $p_K/p_{lg} \approx 0.983$. The adiabatic description of the flow predicts an increase of the mass flux ratio for p_1 approaching p_{lg}. The experimental data shows larger scatter for vapors close to saturation, but hardly an increase of the mass flux ratio.

In Fig. 5, data for $0.2 < \kappa/\kappa_c < 0.4$ is plotted. Under the conditions depicted in Fig. 6, $p_K/p_{lg} \approx 0.965$. Here, the experimental data shows large scatter. For instance, at a value of $p_1/p_{lg} \approx 0.98$ the mass flux ratio lies between values of less than one and about 13. As the scatter in the computed values indicates, the mass flux ratio does not only depend on p_1/p_{lg}. From an analysis of the adiabatic description follows that the mass flux ratio also depends on the pressure difference, see eq. (18) in Ref. [11]. However, the scatter in the experimental data can not be explained by the different pressure differences. The experimental data in Figs. 5 and 6 is color-coded by the pressure difference under which the measurements were taken. Allthough the data points with high mass fluxes in Fig. 5 all have pressure differences smaller than 10 kPa, the data in Figs. 5 and 6 does not allow to draw conclusions regarding the dependency of the accuracy of the measurements on the pressure difference.

Fig. 6 shows a similar picture. For $p_1 < p_K$, the mass flux ratio is close to one. For an upstream state close to saturation, there is considerable scatter in the experimental data. There is one branch with a mass flux ratio smaller than one, and one branch with a mass flux ratio larger than one. Again, the scatter in the calculated values reflects the different conditions under which the measurements were taken.

CONCLUSIONS

The experimental data presented here shows that the flow of vapors through porous membranes can very well be described by the flow of an ideal gas, as long as the permeability of the membrane is larger than the critical permeability κ_c. While the adiabatic description of the flow predicts larger mass fluxes for permeabilities of the membrane which are smaller than the critical permeability, the experimental data suggests that the description of the vapor as an ideal gas is probably correct for permeabilities as small as half the critical permeability.

For smaller permeabilities the experimental data shows large scatter for $p_1 > p_K$. The qualitative agreement with the theoretical description indicates that, for $\kappa/\kappa_c < 0.5$ and $p_1 > p_K$, the vapor condenses fully and liquid flows through a part of the membrane. The poor quantitative agreement probably indicates that the large capillary pressure between the liquid and the vapor phase, which is huge and, hence, has a large influence on the flow, is not correctly described. It may be speculated that the assumption of a constant contact angle is not entirely correct and should be modified.

The qualitative and quantitative disagreement of the isothermal description of the flow and the much better agreement of the adiabatic description with experimental data shows that, when describing a flow with phase changes, the energy balance and probably the Joule-Thomson effect must be considered.

ACKNOWLEDGEMENTS

Financial support by Androsch International Management Consulting GmbH, by the Austrian Exchange Service (Österreichischer Austauschdienst) and by the Czech Science Foundation (Grant No. GA104/09/1165) is gratefully acknowledged.

References

[1] D. A. Nield and A. Bejan, eds. *Convection in Porous Media* (Springer, New York, 2006), 3rd ed.

[2] D. Ingham and I. Pop, eds. *Transport Phenomena in Porous Media III* (Elsevier, Oxford, 2005).

[3] K. Vafai, ed. *Handbook of Porous Media* (Taylor and Francis, New York, 2005), 2nd ed.

[4] W. Schneider. Vapor flow through a porous membrane — a throttling process with condensation and evaporation. *Acta Mech.* **47**, 15–25 (1983).

[5] X. Peng and H. Wu. Pore-scale transport phenomena in porous media. In D. Ingham and I. Pop, eds., *Transport Phenomena in Porous Media III* (Pergamon, Oxford, 2005).

[6] A. Haji-Sheikh and W. J. Minkowycz. Heat Transfer Analysis Under Local Thermal Nonequilibrium Conditions. In P. Vadász, ed., *Emerging Topics in Heat and Mass Transfer in Porous Media* (Springer, New York, 2008).

[7] H. Rhim and S.-T. Hwang. Transport of capillary condensate. *Journal of Colloid and Interface Science* **52**, 174–181 (1975).

[8] K.-H. Lee and S.-T. Hwang. The transport of condensible vapors through a microporous Vycor glass membrane. *Journal of Colloid and Interface Science* **110**, 544–555 (1986).

[9] B. Abeles, L.-F. Chen, J. W. Johnson, and J. M. Drake. Capillary condensation and surface flow in microporous Vycor glass. *Israel Journal of Chemistry* **31**, 99–106 (1991).

[10] P. Uchytil, R. Petrickovic, and A. Seidel-Morgenstern. Study of capillary condensation of butane in a Vycor glass membrane. *Journal of Membrane Science* **264**, 27–36 (2005).

[11] T. Loimer. Linearized description of the non-isothermal flow of a saturated vapor through a micro-porous membrane. *Journal of Membrane Science* **301**, 107–117 (2007).

[12] T. Loimer. Effects of capillarity on a Joule-Thomson process of a fluid near saturation. In Y. Wang and K. Hutter, eds., *Trends in Applications of Mathematics to Mechanics. Proc. 14th STAMM, Aug. 22–28, 2004, Seeheim, Germany*, 247–256 (2005).

[13] J. Roček and P. Uchytil. Evaluation of selected methods for the characterisation of ceramic membranes. *Journal of Membrane Science* **89**, 119–129 (1994).

[14] T. Loimer, P. Uchytil, R. Petrickovic, and K. Setnicková. Isothermal and adiabatic flow of vapors near saturation through porous membranes. In *Eurotherm Seminar Nr. 84, Thermodynamics of phase changes, Namur, Belgium, May 24–27, 2009*. Accepted.